

Hadronic B Decays to Charmless Final States and to $J/\psi K^*$

A. Höcker

Laboratoire de l'Accélérateur Linéaire,
IN2P3-CNRS et Université de Paris-Sud,
BP 34, F-91898 Orsay Cedex, France
E-mail: hoecker@lal.in2p3.fr
(for the BABAR Collaboration)**Abstract**

Preliminary results from the BABAR experiment on charmless B decays to charged pions or kaons, and the measurement of the $B \rightarrow J/\psi K^*$ decay amplitudes are presented. The data sample, collected at the asymmetric-energy B -factory PEP-II at SLAC, comprises a total number of 22.7 million $\Upsilon(4S)$ decays, corresponding to an integrated on-resonance luminosity of approximately 21 fb^{-1} . We measure the following CP -averaged branching fractions: $\mathcal{B}(B^0 \rightarrow \pi^+ \pi^-) = (4.1 \pm 1.0(\text{stat}) \pm 0.7(\text{sys})) \times 10^{-6}$, $\mathcal{B}(B^0 \rightarrow K^+ \pi^-) = (16.7 \pm 1.6(\text{stat})_{-1.7}^{+1.2}(\text{sys})) \times 10^{-6}$, and an upper limit of $\mathcal{B}(B^0 \rightarrow K^+ K^-) < 2.5 \times 10^{-6}$, at 90% confidence limit. The measurement of the $J/\psi K^*$ decay amplitudes results in $R_{\perp} = 0.160 \pm 0.032(\text{stat}) \pm 0.036(\text{sys})$, and reveals a dominant longitudinal component. The phase of the longitudinal amplitude shows evidence for non-vanishing final-state interaction.

Contributed to the Proceedings of the
4th International Conference on B Physics and CP Violation - BCP4
2/13/2000—2/19/2000, Ise-Shima, Japan

Stanford Linear Accelerator Center, Stanford University, Stanford, CA 94309

Work supported in part by Department of Energy contract DE-AC03-76SF00515.

1 Charmless Hadronic B Decays

Hadronic B decays to charmless final states provide a rich environment for CP violation studies as well as searches for new physics. Any $b \rightarrow u\bar{u}d$ transitions, where the hadronic final state may be a CP eigenstate or not, represents a possible source for measuring the angle $\alpha = \arg[-V_{td}V_{tb}^*/V_{ud}V_{ub}^*]$ of the unitarity triangle (UT). Indirect CP violation in $B^0\bar{B}^0$ mixing results from the interference between direct and mixed decays. The weak phase α can be determined from the measurement of the time-dependent asymmetry of $B^0 \rightarrow \pi^+\pi^-$, together with constraints from isospin conservation [1]. Moreover, a three-body Dalitz plot analysis of $B \rightarrow \rho\pi$ decays allows one to simultaneously fit for α and the contributing strong tree and penguin phases [2]. Direct CP violation arises from the interference between tree and penguin amplitudes contributing to the hadronic final state. It can be measured in charged as well as neutral B decays. Several charmless modes are self-tagging which facilitates the search for direct CP violation. Theories employing perturbative QCD [3] or non-leading Factorization Approximation (FA) [4] have been shown to provide predictions of charmless branching fractions of tree and penguins dominated B decay modes. Their measurement can exhibit tests of the theory and may eventually be used to determine the UT angle $\gamma = \arg(V_{ub}^*)$ [5]. Finally, the $B^0 \rightarrow K^+K^-$ branching fraction provides a measure of contributions from W exchange and hard rescattering topologies which are suppressed in the FA.

Preliminary *BABAR* results on charmless B decays using approximately half of the present data set have been presented in Ref. [6]. Significant signals have been found for the modes: $B^0 \rightarrow \pi^+\pi^-$, $B^0 \rightarrow K^+\pi^-$, $B^0 \rightarrow \rho^+\pi^-$ and $B^0 \rightarrow \eta'K$. Updates of these analyses as well as measurements of a large number of new charmless modes are being prepared within the *BABAR* Collaboration. Important activity is also invested into the analyses of $b \rightarrow s\gamma$ decays for which results are forthcoming.

In this note we will concentrate on the measurement of the charged two-body modes $B^0 \rightarrow h^+h'^-$, with $h^{(\prime)}$ being pion or kaon. We use (almost) the full year 1999-2000 data set which amounts to $(22.57 \pm 0.36) \times 10^6$ $B\bar{B}$ pairs, corresponding to an integrated luminosity of approximately 21 fb^{-1} collected by the *BABAR* detector [7] at the PEP-II storage ring. Background studies utilize approximately 3 fb^{-1} of data taken below the $B\bar{B}$ threshold. A “blind” analysis methodology has been adopted throughout, so that the signal region for each mode remained hidden until finalization of event selection and systematic studies.

1.1 $B^0 \rightarrow h^+h'^-$ Candidate Selection

We impose efficient track quality requirements on charged tracks which must have a minimum transverse momentum of $100 \text{ MeV}/c$ in the laboratory frame (LAB). Charged pions and kaons are identified by measuring the Čerenkov angle, θ_C , of photons produced while traversing a radiative medium made of synthetic fused silica, the DIRC [8], surrounding the drift chamber in the barrel [7].

We select $B^0 \rightarrow h^+h'^-$ candidates based on the energy-substituted mass, m_{ES} , where $\sqrt{s}/2$ (\sqrt{s} being the center-of-mass energy) is substituted for the candidate’s energy, and the difference ΔE between the B -candidate energy and $\sqrt{s}/2$. Preselected B candidates are required to satisfy $5.2 < m_{\text{ES}} < 5.3 \text{ GeV}/c^2$ and $|\Delta E| < 0.42 \text{ GeV}$. The dominant background for all charmless modes stems from continuum $q\bar{q}$ production, which exhibits a jet-like structure that distinguishes it from the more spherical topology of generic $B\bar{B}$ events. To suppress this background we use a Fisher discriminant, \mathcal{F} , combining the charged and neutral momentum flow from the rest of the event relative to the candidate’s thrust axis, characterized by nine concentric, 10° wide cones [9].

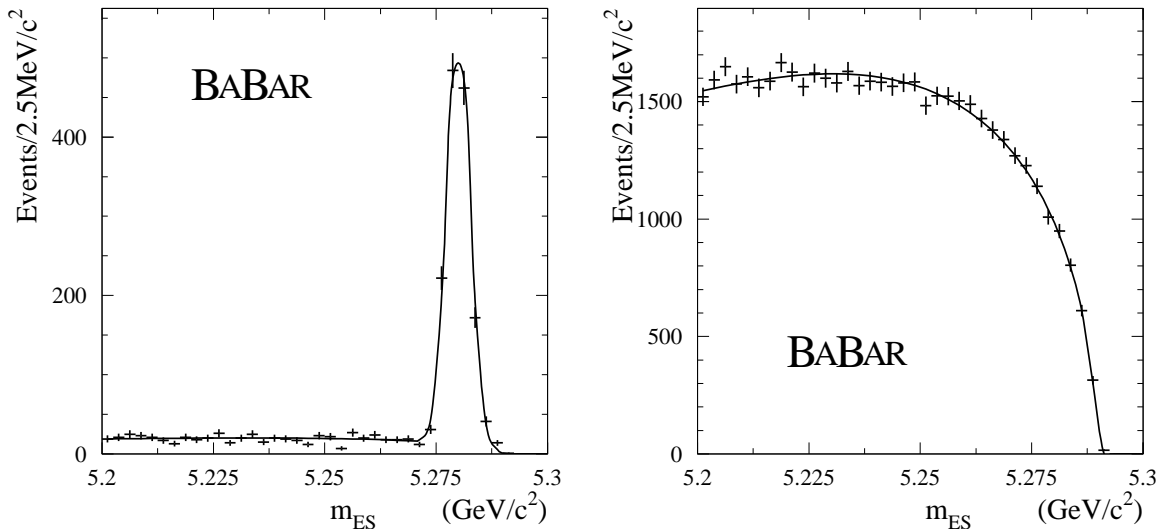


Figure 1: Energy substituted mass spectra. Left: $B^- \rightarrow D^0 \pi^-$ signal with single Gaussian fit. Right: background from ΔE sidebands of $B^- \rightarrow h^+ h'^-$ candidates, fit to an ARGUS shape function [17].

1.2 Calibration of the Discriminating Variables

The signal and background distributions of the discriminating variables are controlled by independent calibration samples obtained from: ΔE and m_{ES} sidebands and off-resonance data to study background characteristics, exclusive $B^- \rightarrow D^0 \pi^- \rightarrow (K^- \pi^+) \pi^+$ decays to gauge the ΔE and m_{ES} resolution of the Monte Carlo (MC) simulation with respect to the data, inclusive $D^{*+} \rightarrow D^0 \pi^+ \rightarrow (K^- \pi^+) \pi^+$ decays to measure the particle identification (PID) performance of the DIRC, and finally MC simulated signal and background events. The calibration measures a m_{ES} resolution of 2.6 MeV/ c^2 for signal events (see Fig. 1 for signal and background distributions), and a ΔE resolution of approximately 26 MeV. The latter value has been rescaled to account for differences between data and MC simulation with a conservative error estimated to be ± 5 MeV. The output of the Fisher discriminant is found to be well reproduced by the MC simulation. A sample of D^* -tagged $D^0 \rightarrow K^- \pi^+$ decays is used to parameterize the θ_C distributions for pion and kaon tracks as a function of the track's polar angle. The K/π separation varies from 2 to more than 8 standard deviations across the relevant momentum range between 1.7 and 4.2 GeV/ c in the LAB.

1.3 Likelihood Fit

Signal yields in all three $h^+ h'^-$ modes are determined simultaneously from an 8 parameter, unbinned maximum likelihood (UML) fit, incorporating m_{ES} , ΔE , \mathcal{F} , and the measured θ_C for each track. All candidates passing the preselection are included in the fit. The probability density function (PDF) for an event i , with a number of signal (background) candidates, $N_{(b)hh'}$, is given by

$$\mathcal{P}_i(\mu) \propto \sum_{h \leq h' = \pi, K} \left(N_{hh'} \mathcal{P}_i^{hh'}(\mu) + N_{bhh'} \mathcal{P}_i^{bhh'}(\mu) \right) + \text{asymmetries} \quad (1)$$

with $(\mu) = (m_{\text{ES}}, \Delta E, \mathcal{F}, \theta_{C,,}^+, \theta_{C,,}^-)$ being the discriminating variables that enter the UML fit. The combined PDF, $\mathcal{P}^{(b)hh'}(\mu)$, is the product of the PDF's of the individual variables. The total extended log-likelihood [10] for N candidates, which is to be maximized in the fit, reads

$$\mathcal{L} = \sum_{i=1}^N \mathcal{P}_i(\mu) - N', \quad (2)$$

where $N' = \sum_{h,h'} (N_{h,h'} + N_{bh'h'})$ is the Poissonian extension of the likelihood. A bias, enhancing the contributions from $\pi^+\pi^-$ and K^+K^- with respect to $K^+\pi^-$, has been identified in the 6 parameter UML fit previously applied [6]. This was due to the implicit assumption of randomly paired background tracks. The addition of 2 independent background parameters provides the remedy to the problem.

1.4 Systematic Uncertainties

Systematics uncertainties arise from the imperfect knowledge of the PDF shape parameterizations. Associated errors are quantified by varying the parameters within their statistical errors and to cover disagreements between MC and data. Alternate parameterizations are used in addition. A large number of cross checks have been performed to validate the fit procedure. Toy MC studies showed no bias in the fit outputs. A cut-based analysis, performed in parallel, agrees with the results from the UML fit.

1.5 Results

With signal efficiencies of $\epsilon_{\pi\pi} = 0.448 \pm 0.008$, $\epsilon_{K\pi} = 0.447 \pm 0.008$ and $\epsilon_{KK} = 0.429 \pm 0.008$, we find signal yields $N_{\pi\pi} = 41 \pm 10 \pm 7$, $N_{K\pi} = 169 \pm 17^{+12}_{-17}$ and $N_{KK} = 8.2^{+7.8}_{-6.4} \pm 3.3$, from the likelihood fit, where the uncertainties are statistical and systematic. The correlations between these numbers are below 15%. The systematic errors are dominated by the uncertainties in the description of \mathcal{F} and the resolution on ΔE . Figure 2 shows the m_{ES} distributions for candidates of the three final states from the cut based analysis.

The branching fractions are obtained from the signal yield *via* $\mathcal{B}(B \rightarrow h^+h'^-) = N_{hh'}/(\epsilon_{hh'} N_{B\bar{B}})$, giving

$$\mathcal{B}(B^0 \rightarrow \pi^+\pi^-) = (4.1 \pm 1.0 \pm 0.7) \times 10^{-6}, \quad (3)$$

$$\mathcal{B}(B^0 \rightarrow K^+\pi^-) = (16.7 \pm 1.6^{+1.2}_{-1.7}) \times 10^{-6}, \quad (4)$$

$$\mathcal{B}(B^0 \rightarrow K^+K^-) < 2.5 \times 10^{-6} \quad (90\% \text{ CL}), \quad (5)$$

where the uncertainties are statistical and systematic. The statistical significance is 4.7 (15.8) standard deviations for the $\pi^+\pi^-$ ($K^+\pi^-$) final state. We do not find a significant signal yield in the mode $B^0 \rightarrow K^+K^-$ and hence quote an upper limit at 90% confidence level. The results are consistent with our previous preliminary numbers [6], based on less than half the present data set. A comparison with published branching ratios from CLEO [11] and preliminary results from BELLE [12] is given in Fig. 3, showing consistency.

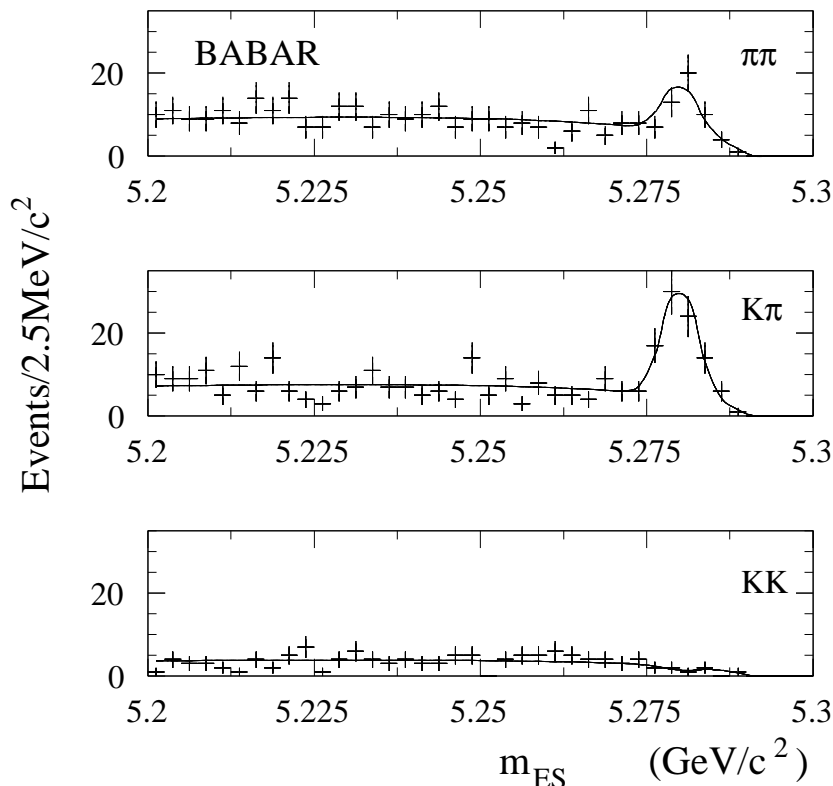


Figure 2: Distribution of m_{ES} for the B^0 final states $\pi^+\pi^-$ (upper plot), $K^+\pi^-$ (middle plot) and K^+K^- (lower plot), from the cut based analysis.

2 Measurement of the $B \rightarrow J/\psi K^*$ Decay Amplitudes

The decay $B^0 \rightarrow J/\psi K^{*0}$, $K^{*0} \rightarrow K_S^0 \pi^0$ can be used in time dependent CP asymmetry studies to measure the CP violating parameter $\sin 2\beta$. In contrast to the pure CP -odd eigenstate $B^0 \rightarrow J/\psi K_S^0$, this pseudoscalar to vector-vector decay gives a mixture of CP -odd and CP -even eigenstates since orbital angular momenta $L = 0, 1, 2$ of the $(J/\psi, K^{*0})$ system are allowed. If one CP contribution dominates, $\sin 2\beta$ can be measured as in the $B^0 \rightarrow J/\psi K_S^0$ case, using the time distribution only. Otherwise, both the angular and time distributions are needed to avoid a partial cancellation of the observed CP asymmetry [13]. Assuming the weak decay to be isospin invariant, the amplitudes can be measured using all $K^* \rightarrow K\pi$ modes, which greatly increases statistics.

Three amplitudes are necessary to describe the decay. In the transversity basis [13, 14], used in previous analyses by CLEO [15] and CDF [16], the amplitudes A_{\parallel} , A_0 and A_{\perp} , have definite CP eigenvalues: the latter is CP -odd and the former two are CP -even. The longitudinal polarization fraction of the decay is measured by $|A_0|^2 \equiv \Gamma_L/\Gamma$, whereas A_{\parallel} and A_{\perp} govern the transverse polarization and correspond to parallel and perpendicular polarizations of the two vector mesons, respectively. Hence, $|A_{\perp}|^2$ measures the P wave contribution to the decay. The measurement of the decay amplitudes also provides a test of the factorization hypothesis. In the factorization scheme, the weak decay is described by a product of two hadronic currents, J/ψ and $B \rightarrow K^*$, where

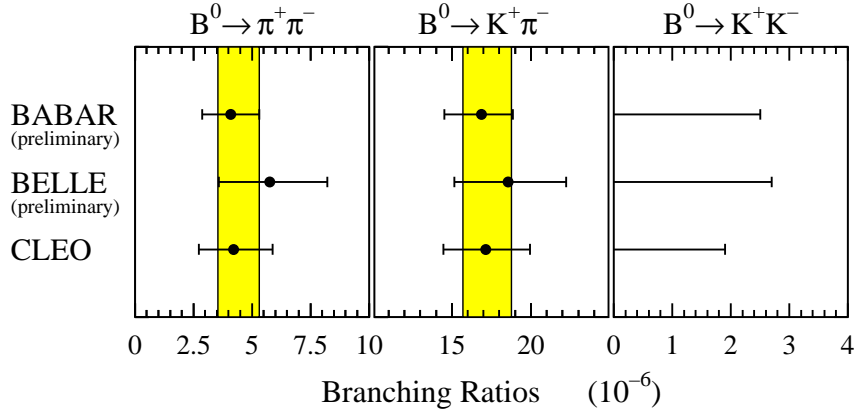


Figure 3: Comparison of measured branching ratios to h^+h^- final states. The shaded bands give the averages for the significant measurements.

final-state interaction is neglected. If factorization holds, the corresponding amplitudes should have trivial relative phases of 0 or π .

We present preliminary results on a complete angular analysis in the transversity basis considering the decays $B^0 \rightarrow J/\psi K^{*0}$ and $B^+ \rightarrow J/\psi K^{*+}$, where the K^{*0} and K^{*+} are reconstructed in the modes $K_S^0 \pi^0$, $K^+ \pi^-$ and $K_S^0 \pi^+$ and $K^+ \pi^0$, the K_S^0 decaying into two charged pions, and the J/ψ through decays into e^+e^- and $\mu^+\mu^-$. The data sample used corresponds to the full year 1999-2000 recording of $(22.7 \pm 0.4) \times 10^6$ $B\bar{B}$ pairs (see Section 1).

2.1 $B \rightarrow J/\psi K^*$ Candidate Selection

Charged tracks are used in a fiducial polar angle range where PID efficiencies are well understood. Electrons are identified requiring their momentum to be compatible with their energy deposition in the electromagnetic calorimeter (EMC), and their dE/dx to be compatible with the electron hypothesis. Muons are required to penetrate at least 2 interaction lengths in the detector and to leave a low number of hits per layer in the Instrumented Flux Return (IFR). If a muon penetrates the EMC, it is required to deposit energy consistent with a minimum ionizing particle. Kaon candidates are required to pass a pion veto based on DIRC and dE/dx information.

J/ψ candidates are selected requiring both leptons to be identified. The vertexed lepton pair is required to have an invariant mass in the range 3.06-3.14 GeV/c^2 for muons and 2.95-3.14 GeV/c^2 for electrons. K_S^0 are reconstructed as vertexed pairs of charged tracks with an invariant mass between 489 and 507 MeV/c^2 and a flight direction which is compatible to originate from the interaction point. Photons are defined as neutral clusters with an energy greater than 30 MeV and photon-like shower shapes. Neutral pions are selected from pairs of photons with an invariant mass between 106 and 153 MeV/c^2 . The J/ψ , K_S^0 and π^0 are fitted to their respective nominal masses. K^* are formed as $K\pi$ combinations with an invariant mass within ± 100 MeV/c^2 of the nominal $K^*(892)$ mass.

Finally, B mesons are formed by combining J/ψ and K^* candidates. Furthermore, requirements

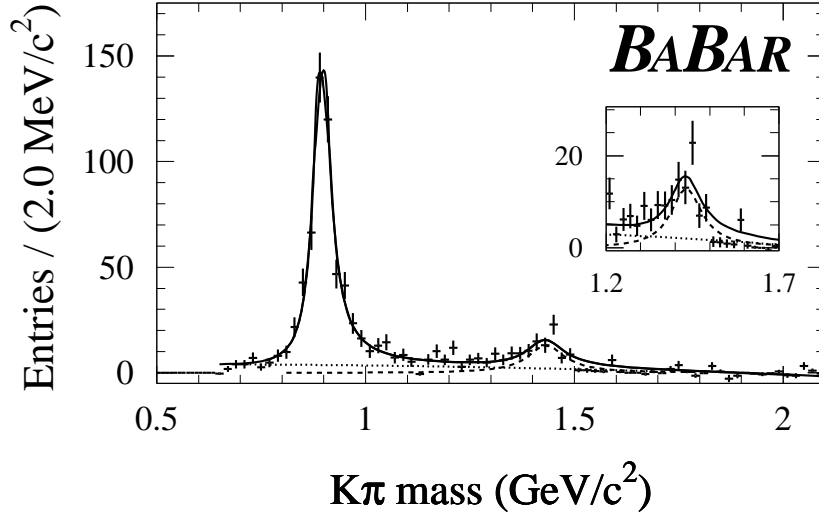


Figure 4: Background-subtracted $K\pi$ mass distribution in the mode $B^0 \rightarrow J/\psi K^{*0}$, $K^{*0} \rightarrow K^\pm \pi^\mp$.

on the cosine of the K^* helicity angle reduce the cross feed (CF) from $J/\psi(K\pi^\pm)^*$ modes, where the π^\pm is lost, and the self cross feed (SCF) due to a wrongly reconstructed π^0 picked up by the reconstruction. The (S)CF is the most important background and accumulates in the m_{ES} signal region. B meson candidates are selected with ΔE (required to be between -70 MeV and $+50$ MeV for channels involving a π^0 and within ± 30 MeV in the other cases) and m_{ES} . For the m_{ES} signal region between 5.27 and 5.29 GeV/c^2 we obtain reconstruction efficiencies of 9.9%, 23.9%, 17.2% and 13.8% for the $J/\psi K_S^0 \pi^0$, $J/\psi K^+ \pi^-$, $J/\psi K_S^0 \pi^+$ and $J/\psi K^+ \pi^0$ modes, respectively. The corresponding (S)CF contamination amounts to (1.6)15.8%, (0.6)2.4%, (0.5)3.0% and (2.2)15.7% of the signal contributions. The signal yields are obtained by a fit of the m_{ES} spectra describing the background by an ARGUS function [17] and the signal by a Gaussian: $N(J/\psi K_S^0 \pi^0) = 39 \pm 6$, $N(J/\psi K^+ \pi^-) = 530 \pm 32$, $N(J/\psi K_S^0 \pi^+) = 131 \pm 12$ and $N(J/\psi K^+ \pi^0) = 195 \pm 15$.

As shown in Ref. [15], $K\pi$ production other than *via* the $K^*(892)$ contributes to $B \rightarrow J/\psi K\pi$ final states. Figure 4 shows the $K\pi$ mass distribution for the $B \rightarrow J/\psi K^\pm \pi^\mp$ mode, after subtraction of combinatoric $K\pi$ background from the low m_{ES} region. We observe clear evidence of resonant excitation around 1430 MeV/c^2 .

2.2 Angular Distribution and Fitting Method

The transversity frame is defined in the J/ψ rest frame. The K^* direction defines the $-x$ axis. The $K\pi$ plane defines the (x, y) plane, with y such that $p_y(K) > 0$. The z axis is normal to that plane so that the (x, y, z) frame is right handed. The transversity angles θ_{tr} and ϕ_{tr} are defined as the polar and azimuthal angles of the ℓ^+ originating from the J/ψ . The K^* helicity angle θ_{K^*} is the angle between the K direction and the direction opposite to the J/ψ in the K^* rest frame. Defining:

$$f_1 = + 9/(32\pi) \cdot 2 \cos^2 \theta_{K^*} (1 - \sin^2 \theta_{tr} \cos^2 \phi_{tr})$$

$$\begin{aligned}
f_2 &= + 9/(32\pi) \cdot \sin^2 \theta_{K^*} (1 - \sin^2 \theta_{\text{tr}} \sin^2 \phi_{\text{tr}}) \\
f_3 &= + 9/(32\pi) \cdot \sin^2 \theta_{K^*} \sin^2 \theta_{\text{tr}} \\
f_4 &= + 9/(32\pi) \cdot \sin^2 \theta_{K^*} \sin 2\theta_{\text{tr}} \sin \phi_{\text{tr}} \cdot \zeta \\
f_5 &= - 9/(32\pi) \cdot 1/\sqrt{2} \cdot \sin 2\theta_{K^*} \sin^2 \theta_{\text{tr}} \sin 2\phi_{\text{tr}} \\
f_6 &= + 9/(32\pi) \cdot 1/\sqrt{2} \cdot \sin 2\theta_{K^*} \sin 2\theta_{\text{tr}} \cos \phi_{\text{tr}} \cdot \zeta ,
\end{aligned}$$

the angular distribution $g(\cos \theta_{\text{tr}}, \cos \theta_{K^*}, \phi_{\text{tr}})$ reads

$$\begin{aligned}
g &= \frac{1}{\Gamma} \frac{d^3\Gamma}{d\cos \theta_{\text{tr}} d\cos \theta_{K^*} d\phi_{\text{tr}}} \\
&= f_1 |A_0|^2 + f_2 |A_{\parallel}|^2 + f_3 |A_{\perp}|^2 + f_4 \text{Im}(A_{\parallel}^* A_{\perp}) + f_5 \text{Re}(A_0^* A_{\parallel}) + f_6 \text{Im}(A_0^* A_{\perp}) .
\end{aligned} \tag{6}$$

The parameter ζ is +1 for B^+ and B^0 and -1 for B^- and \bar{B}^0 . For the CP eigenstate $K_S^0 \pi^0$, a $B^0 \bar{B}^0$ from the decay of an $\Upsilon(4S)$ has $\zeta = \pm 1/(1 + x_d^2)$. However, the initial B^0 flavor is not determined in this analysis so the appropriate value for ζ is the average, namely zero.

The amplitudes are fitted by means of a UML fit exploiting the angular and m_{ES} information. All B candidates within $5.2 < m_{\text{ES}} < 5.3 \text{ GeV}/c^2$ enter the fit, where the m_{ES} sidebands are used to normalize non $B \rightarrow J/\psi K^*$ background. The biases on the amplitudes due to limited acceptance and background are corrected considering only the projections on the basis of the f_i 's [18].

Signal events are described by the PDF

$$g_{\text{obs}} = g(\vec{\omega}_j) \times \epsilon(\vec{\omega}_j) / \langle \epsilon \rangle , \tag{7}$$

where $\vec{\omega}_j$ stands for the three angles of the observed event j , and $\epsilon(\vec{\omega}_j)$ is the efficiency for this event. Rewriting Eq. (6) as $g = \sum_{i=1}^6 f_i A_i^2$, where the A_i^2 ($i = 1, 6$) are $|A_0|^2$, $|A_{\parallel}|^2$, $|A_{\perp}|^2$, $\text{Im}(A_{\parallel}^* A_{\perp})$, $\text{Re}(A_0^* A_{\parallel})$ and $\text{Im}(A_0^* A_{\perp})$, the mean efficiency $\langle \epsilon \rangle$ reads

$$\langle \epsilon \rangle = \int g \times \epsilon = \sum_{i=1}^6 A_i^2 \xi_i , \tag{8}$$

where the $\xi_i = \int f_i \times \epsilon$ are amplitude independent. The signal part of the log-likelihood

$$\mathcal{L}_{\text{signal}} = \sum_{j=1}^{N_{\text{obs}}} \log (g_{\text{obs}}(\vec{\omega}_j)) , \tag{9}$$

where N_{obs} is the number of observed events, becomes

$$\mathcal{L}_{\text{signal}} = \sum_{j=1}^{N_{\text{obs}}} \log (g(\vec{\omega}_j)) + \sum_{j=1}^{N_{\text{obs}}} \log (\epsilon(\vec{\omega}_j)) - N_{\text{obs}} \log \left(\sum_{i=1}^6 A_i^2 \xi_i \right) . \tag{10}$$

Since the $\epsilon(\vec{\omega}_j)$ do not depend on the amplitudes, the term $\sum_{j=1}^{N_{\text{obs}}} \log(\epsilon(\vec{\omega}_j))$ is left out: detailed knowledge of the acceptance is not necessary in this approach.

The coefficients ξ_i are evaluated using a detailed simulation of the *BABAR* detector. Separate series of ξ_i 's are used for each $B \rightarrow J/\psi K^*$ channel. The values found for ξ_i , ($i = 1, 3$), are close to the efficiency of the final state, with a lower value for ξ_1 , especially in modes involving π^0 , due to the

Table 1: Systematic uncertainties. Details are given in the text.

	$ A_0 ^2$	$ A_\perp ^2$	$ A_\parallel ^2$	ϕ_\perp	ϕ_\parallel
MC stat.	0.006	0.006	0.007	0.04	0.06
Backgr.	0.002	0.005	0.006	0.01	0.00
Track. & PID	0.002	0.006	0.004	0.00	0.02
Heavy K^*	0.005	0.035	0.031	0.04	0.02
Total	0.008	0.036	0.033	0.06	0.07

Table 2: Preliminary amplitude moduli-squared and phases. The uncertainties are statistical and systematic.

Quantity	Value
$ A_0 ^2$	$0.597 \pm 0.028 \pm 0.008$
$ A_\perp ^2$	$0.160 \pm 0.032 \pm 0.036$
$ A_\parallel ^2$	$0.243 \pm 0.034 \pm 0.033$
$\phi_\perp = \arg(A_\perp/A_0)$	$-0.17 \pm 0.16 \pm 0.06$
$\phi_\parallel = \arg(A_\parallel/A_0)$	$2.50 \pm 0.20 \pm 0.07$

requirement on $\cos\theta_{K^*}$. The ξ_i , ($i = 4, 6$), are compatible with zero.

The PDF of the non $B \rightarrow J/\psi K^*$ background $g_B^{\text{obs}}(\vec{\omega}_j)$ is written as a distribution g_B of amplitudes B_i^2 ($i = 1, 6$): $g_B^{\text{obs}}(\vec{\omega}_j) = g_B(\vec{\omega}_j) \times \epsilon(\vec{\omega}_j)/\langle\epsilon\rangle$. The shape and level of the (S)CF background is amplitude dependent. The bias due to (S)CF background can be corrected by a modification $\tilde{\xi}_i$ of the ξ_i , obtained by integrating, in addition to the signal as before, over the (S)CF contributions. In contrast to ξ_i , the $\tilde{\xi}_i$ depend on the amplitudes used in the simulation. The maximum bias on the fitted amplitudes was found to be a few parts per thousand.

Finally, the complete log-likelihood has the form

$$\mathcal{L} = \sum_{j=1}^{N_{\text{obs}}} \log \left(x \cdot G(m_{\text{ES}j})g(\vec{\omega}_j) + (1-x) \cdot B(m_{\text{ES}j})g_B(\vec{\omega}_j) \right) - N_{\text{obs}} \log \left(\sum_{i=1}^6 \tilde{\xi}_i \left(x \cdot A_i^2 + (1-x) \cdot B_i^2 \right) \right) - \mathcal{N} ,$$

where $G(m_{\text{ES}})$ and $B(m_{\text{ES}})$ are the Gaussian signal function and ARGUS background function, respectively. The parameter x measures the signal fraction. The normalization of the amplitudes is enforced by the likelihood extension $\mathcal{N} = N_{\text{obs}}(|A_0|^2 + |A_\parallel|^2 + |A_\perp|^2)$.

2.3 Systematic Uncertainties

The limited MC statistics (32000 events per channel) gives rise to a systematic uncertainty on acceptance and cross feed corrections. A fraction of the feed-across background may be absorbed

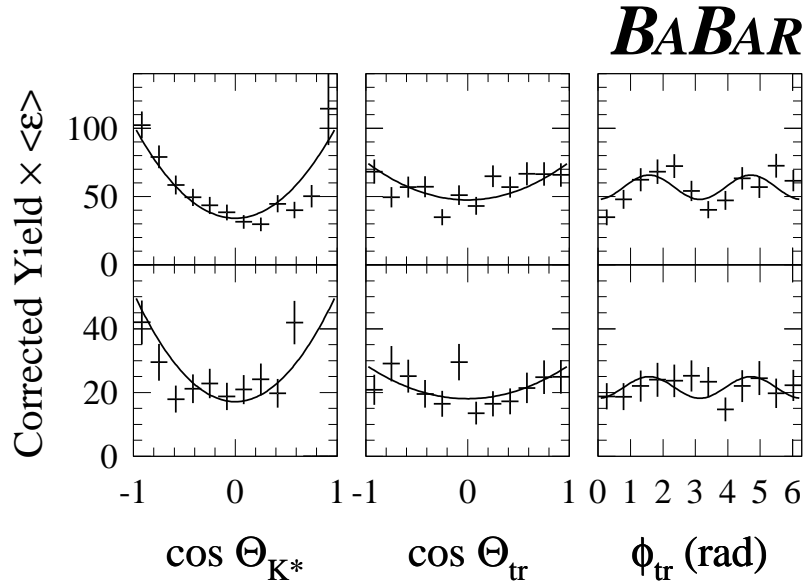


Figure 5: One-dimensional projections of the three transversity angles. The result of the fit is superimposed. The data are corrected for bin-by-bin acceptance. Top plot: modes without π^0 in the final state, and bottom plot: modes with π^0 .

in the fit by the non $B \rightarrow J/\psi K^*$ background component. The size of this effect is evaluated on MC samples, where a set of fits are performed with the non- $J/\psi K^*$ background (ARGUS) function removed. The largest deviation found is taken as an estimate of the associated systematic uncertainty. Discrepancies between the true detector and the simulation affect the acceptance correction. The scale of the effect is estimated by varying the tracking and particle identification efficiencies at MC level. Non-resonant $K\pi$ combinations, higher mass $K\pi$ resonances and their interference with the $K^*(892)$ can contribute to the events in the K^* mass window. The size of the potential bias from these events is estimated by the magnitude of the shift in the fitted angular amplitudes when events in the region $|m_{K\pi} - 1.2| < 0.1 \text{ GeV}/c^2$ are included in the fit.

Table 1 quantifies the systematic effects of the contributions listed above on the fit observables.

2.4 Results

The UML fit results for amplitude moduli-squared and phases are given in Tab. 2. The errors account for statistical and systematic uncertainties. One-dimensional projections of the fitted amplitude spectrum on the three transversity angles are shown in Fig. 5 for modes without π^0 (upper plots) and with π^0 (lower plots) in the final states. Figure 6 visualizes the quantitative effects of the different corrections on the amplitude moduli-squared. Only the acceptance correction exceeds the range defined by the statistical uncertainties. Figure 7 shows the comparison between this preliminary measurement and results from BELLE [19] (preliminary), CDF [16] and CLEO [15], which are found to be consistent. The shaded bands indicate the weighted averages. The *BABAR* values improve the precision by about a factor of two.

We find a dominant longitudinal component and a small P wave contribution. If $\sin 2\beta$ is measured

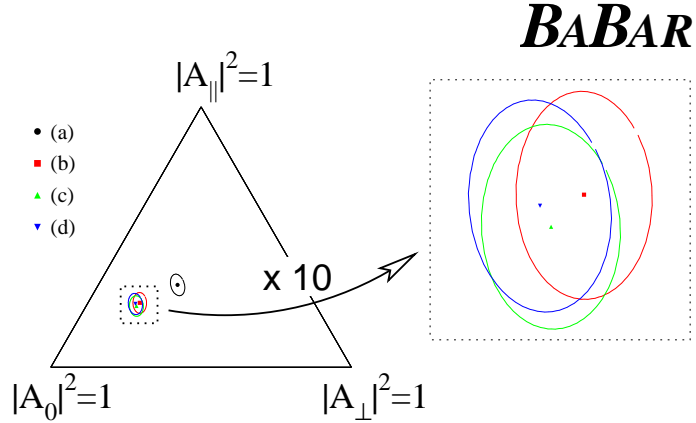


Figure 6: Results of the amplitude fits and effects of the corrections applied. The results are shown in the allowed domain of the amplitude moduli-squared defined by the conditions $|A_0|^2 + |A_||^2 + |A_⊥|^2 = 1$ and $|A_i|^2 \geq 0, (i = 0, ||, \perp)$. Left: the entire allowed domain, right: zoom by a factor of ten into the (b, c, d) region. (a), angular fit with no acceptance correction or m_{ES} dependence, (b), acceptance correction applied, (c), m_{ES} dependence added, and (d), (S)CF correction added.

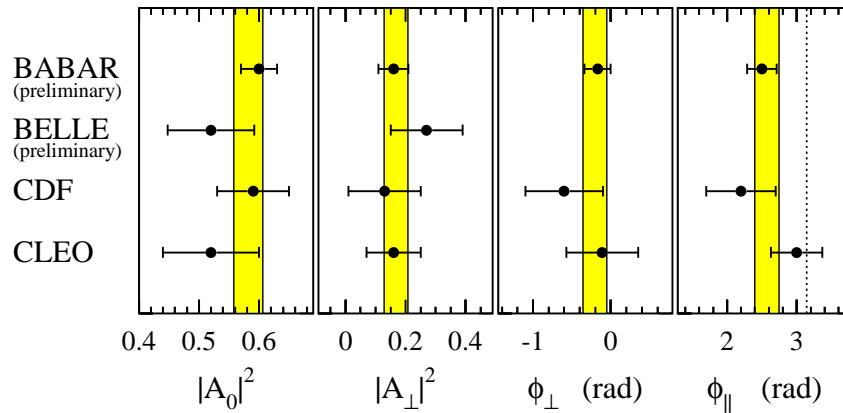


Figure 7: Comparison of measured amplitude moduli-squared and phases (see text for references). The Belle fit assumed no final-state interaction. The shaded bands give the averages.

from a time dependent CP asymmetry analysis in the mode $B \rightarrow J/\psi K_S^0 \pi^0$, the dilution introduced amounts to $D_{\perp} = (1 - 2|A_{\perp}|^2) = 0.68 \pm 0.10$. The uncertainty on $|A_{\perp}|^2$ contributes with relative 14% to the total error of $\sin 2\beta$. This measurement of ϕ_{\parallel} implies a deviation from π by 3 standard deviations (3.4 for the world average), and thus represents evidence for non-vanishing final-state interaction.

Acknowledgements

I am indebted to all my *BABAR* colleagues who helped me preparing this talk. Many thanks to the experts D. Bernard, G. Cavoto, C. Dallapiccola, J. Olsen and M. Verderi for their knowledgeable comments on the analyses reported here. We are grateful for the contributions of our PEP-II colleagues in achieving the excellent luminosity and machine conditions that have made this work possible. We acknowledge support from the Natural Sciences and Engineering Research Council (Canada), Institute of High Energy Physics (China), Commissariat à l’Energie Atomique and Institut National de Physique Nucléaire et de Physique des Particules (France), Bundesministerium für Bildung und Forschung (Germany), Istituto Nazionale di Fisica Nucleare (Italy), The Research Council of Norway, Ministry of Science and Technology of the Russian Federation, Particle Physics and Astronomy Research Council (United Kingdom), the Department of Energy (US), and the National Science Foundation (US). In addition, individual support has been received from the Swiss National Foundation, the A. P. Sloan Foundation, the Research Corporation, and the Alexander von Humboldt Foundation. The visiting groups wish to thank SLAC for the support and kind hospitality extended to them.

References

- [1] M. Gronau and D. London, *Phys. Rev. Lett.* **65**, 3381 (1990)
- [2] H.R. Quinn and A.E. Snyder, *Phys. Rev. D* **48**, 2139 (1993)
- [3] Y.Y. Keum, H.N. Li, C. Kung and A.I. Sanda, *Phys. Rev. D* **63**, 054008 (2001)
- [4] M. Beneke, G. Buchalla, M. Neubert and C.T. Sachrajda, *Nucl. Phys. B* **591**, 313 (2000)
- [5] R. Fleischer, *Phys. Lett. B* **365**, 399 (1996); R. Fleischer and T. Mannel, *Phys. Rev. D* **57**, 2752 (1998)
- [6] T.J. Champion (*BABAR* Collaboration), SLAC-PUB-8696, *BABAR-PROC-00/13*, 2000
- [7] *BABAR* Collaboration, B. Aubert *et al.*, *BABAR-CONF-00/15*, submitted to the XXXth ICHEP’2000, Osaka, Japan, 2000
- [8] B. Ratcliff, SLAC-PUB-5946 (1992), SLAC-PUB-6067 (1993); P. Coyle *et al.*, *Nucl. Instrum. Methods A* **343**, 292 (1993)
- [9] CLEO Collaboration, D.M. Asner *et al.*, *Phys. Rev. D* **53**, 1039 (1996)
- [10] R. Barlow, *Nucl. Instrum. Methods A* **297**, 496 (1990)
- [11] CLEO Collaboration, A. Cronin-Hennesy *et al.*, *Phys. Rev. Lett.* **85**, 515 (2000)

- [12] T. Iijima (BELLE Collaboration), “*B meson rare decays*”, Talk given at BCP4, Ise-Shima, Japan, 2001
- [13] I. Dunietz *et al.*, *Phys. Rev. D* **43**, 2193 (1991)
- [14] A.S. Dighe, I. Dunietz, H.J. Lipkin and J.L. Rosner, *Phys. Lett. B* **369**, 144 (1996)
- [15] CLEO Collaboration, C.P. Jessop *et al.*, *Phys. Rev. Lett.* **79**, 4533 (1997)
- [16] CDF Collaboration, T. Affolder *et al.*, *Phys. Rev. Lett.* **85**, 4668 (2000)
- [17] ARGUS Collaboration, H. Albrecht *et al.*, *Z. Phys. C* **48**, 543 (1990)
- [18] S. Ferrag, PhD Thesis (*in preparation*), Ecole Polytechnique, France, 2001
- [19] BELLE Collaboration, A. Abasian *et al.*, BELLE-CONF-0014, submitted to the XXXth ICHEP’2000, Osaka, Japan, 2000